Compound-nucleus contribution to (α, α') reactions in Ni, Zn, and Sn†

J. E. Alzona, K. C. Chan, L. Shabason, and B. L. Cohen
Nuclear Physics Laboratory, University of Pittsburgh, Pittsburgh, Pennsylvania 15260
(Received 3 February 1975)

A clean separation of compound nucleus from noncompound nucleus processes in (α, α') reactions is made for 18-MeV α-particles on Ni, Zn, and Sn. Experimental results agree well with both Weisskopf and Hauser-Feshbach theory using Gilbert-Cameron level densities. In addition, a surprising theoretical prediction in the case of Ni is dramatically confirmed by experiment.

[NUCLEAR REACTIONS ^{58,60,62}Ni(α, α'), ^{64,66}Zn(α, α'), ^{112}Sn(α, α'), $E = 18$ MeV; measured $d^2\sigma/d\Omega dE$, deduced compound-nucleus contribution to cross section, compared with calculations from Weisskopf, Hauser-Feshbach statistical theory.]

I. INTRODUCTION

In this paper we separate compound-nucleus (CN) contributions from non-compound-nucleus contributions to the cross section for (α, α') reactions on the even isotopes of Ni, Zn, and Sn at 18-MeV incident energy, and analyze these CN contributions. Our method has been previously applied to (p, p'), (α, p), and (p, α) reactions,[1] and except for the last case, good agreement was found with statistical theory calculations based on Gilbert-Cameron level densities. In (p, α) reactions, however, although shapes of the CN spectra were found to be in reasonably good agreement with statistical theory, the measured absolute cross sections differed from calculated cross sections by up to a factor of 10, the greatest discrepancies being for the heavier isotopes. To a large extent, these discrepancies in the case of (p, α) reactions as opposed to good agreement in both (p, p') and (α, p) are what motivated the present (α, α') studies.

II. EXPERIMENTAL

A block diagram of the experimental arrangement used is shown in Fig. 1. 18-MeV α particles were obtained from the University of Pittsburgh Van de Graaff accelerator and collimated by a circular slit 0.63 cm in diameter 10.2 cm in front of the target. The targets were self-supporting foils of isotopes of Ni, Zn, and Sn with thicknesses ranging from 0.5 to 2.5 mg/cm^2, most of them having thicknesses of approximately 1 mg/cm^2. These target thicknesses were obtained to an accuracy of about 5% by measuring the energy lost by the 5.48-MeV α particles from ^{241}Am in passing through these targets. As a check against nonuniformity in target thicknesses, two scintillation detectors located at 25° on either side of the beam were used as monitors detecting elastically scattered α particles. The emitted α particles were detected by two telescopes set at different angles, each telescope consisting of two surface barrier charged particle detectors. The ΔE front detectors and E back detectors were 50 μm and 2000 μm thick, respectively. Initial runs were made at laboratory angles of 75° and 135°, but α-particle groups emitted from carbon and oxygen impurities proved to be particularly troublesome at 75°, so later runs were made at laboratory angles of 95° and 135°. These impurity-caused α-particle groups are then easily subtracted off by comparison with spectra from Mylar targets. Typical beam currents were 100 nA; the undeflected beam was collected in a Faraday cup, and the total charge collected was used to obtain absolute cross sections.

III. THEORY AND RESULTS

A. Sn isotopes

Since the theoretical basis for the method used in separating the CN from the non-CN processes has been discussed fully elsewhere,[1] we present only the salient points as applied to the Sn isotopes. The method takes advantage of the fact that for CN reactions, the (α, α') reaction channel competes less and less effectively with the (α, n) channel as we go to heavier isotopes of the same element. This is reflected in the reaction Q values $Q(\alpha, n)$ (Table II and Fig. 2). Thus cross sections for CN reactions in the heavier isotopes are usually orders of magnitude less than in the lighter isotopes (Fig. 2). On the other hand, cross sections for direct reactions depend on the structure of the ground and excited states of nuclei; thus it is reasonable to assume that all the even-even isotopes

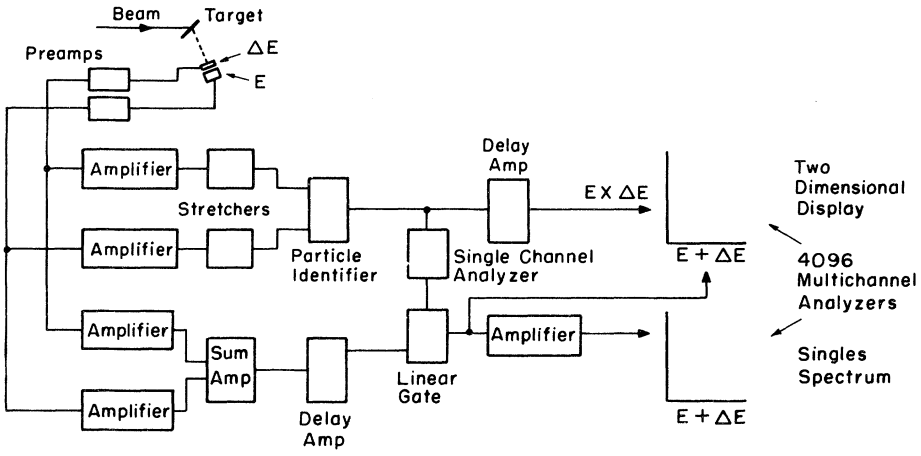

FIG. 1. Electronics used in the experiment.

of the same element have about the same direct reactions. The correctness of this assumption in the case of the Sn isotopes is supported by the experimental fact that the spectra for all the Sn isotopes except ^{112}Sn have practically the same value (Fig. 3), which we take to be essentially the direct reactions. This strongly suggests that of the even Sn isotopes, only ^{112}Sn has an appreciable CN contribution to its (α, α') spectrum, and this CN contribution is obtained by subtracting out the direct reaction part from the total reaction cross section for ^{112}Sn.

To obtain the theoretical curves, we used both the code and optical model parameters of Perey[2] to calculate neutron and proton total reaction cross sections; α-particle optical model parameters are those of McFadden and Satchler[3] with an extrapolation for the imaginary volume potential; using Gilbert-Cameron level density parameters,[4] we then did statistical theory calculations according to both the Weisskopf [Eq. (1)] and the Hauser-Feshbach angular-momentum dependent theory [Eq. (2)]; in both cases we took the cross section for the *formation* of the compound nucleus $\sigma_{CN}(\alpha)$ to be 80% of the total reaction cross section generated by the optical model codes mentioned above,

TABLE I. Optical potential parameters used in this paper; E is the projectile energy in MeV. In all cases the real and imaginary parts of the Woods-Saxon potential were assumed to have the same shape. $r_{Coul} = 1.30$ fm.

Element	V (MeV)	W (MeV)	r_0 (fm)	a (fm)
Ni	198.6	$0.61(E+8.0)$	1.458	0.502
Zn	193.4	$0.74(E+8.0)$	1.435	0.521
Sn	219.3	$0.97(E+8.0)$	1.395	0.549

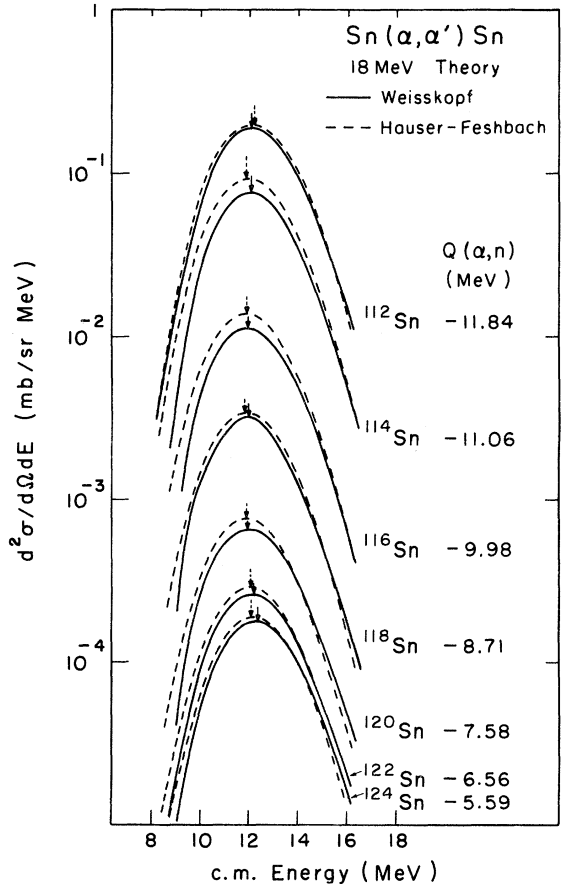

FIG. 2. Theoretical curves (α, α') CN cross sections for the Sn isotopes. The reaction Q values $Q(\alpha, n)$ for each Sn isotope are also shown on the right. Arrows point out the position of the peak for each spectrum. "c.m. Energy" means energy of the outgoing α particle in the center-of-mass frame.

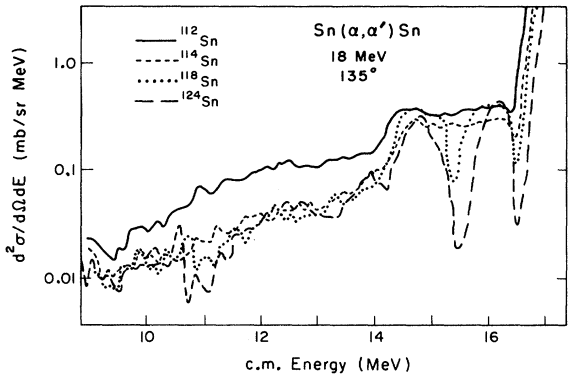

FIG. 3. Raw experimental spectra for the Sn isotopes. The curves for ^{116,120,122}Sn are not included for the sake of clarity of the diagram, but they all have essentially the same value as the ^{114,118,124}Sn curves shown above.

exactly as was done in previous papers. Weisskopf angular-momentum-averaged statistical theory[5] gives

$$\frac{d^2\sigma}{dEd\Omega} = \frac{\sigma_{CN}(\alpha)}{4\pi}\frac{2M_\alpha}{\hbar^2}(2S_\alpha+1)\frac{\sigma_\alpha(E)E\omega(E_{by}-E)}{F_n+F_p+F_\alpha}, \tag{1}$$

where

$$F_b(E_{by}) = \frac{2M_b}{\hbar^2}(2S_b+1) \times \int_0^{E_{by}} \sigma_b(\epsilon_\beta)\epsilon_\beta\omega(E_{by}-\epsilon_\beta)d\epsilon_\beta$$

for the CN reaction $X(a,b)Y^*$, M_b and S_b are, respectively, the mass and spin of b, $\sigma_b(\epsilon_\beta)$ is the inverse cross section, E_{by} is the maximum available energy, $(E_{by}-\epsilon_\beta)$ is the excitation energy of the residual nucleus Y^*, and ω are the Gilbert-Cameron composite level densities.

Hauser-Feshbach angular-momentum dependent statistical theory[6] gives

$$\frac{d^2\sigma}{dEd\Omega} = (k_\alpha\hat{I}_1\hat{i}_1)^{-2} \times \sum_{\substack{S_1,S_2I_2\\ L\ \text{even}}} B_L(E,S_1,S_2)P_L(\cos\theta)\omega(E_{by}-E,I_2), \tag{2}$$

where k_α is the wave number of the incident α particle; I_1 and i_1 refer to target and projectile spins; I_2 and i_2 refer to residual nucleus and emitted particle spins; $S=I+i$ is the channel spin; $J=S+l$ is the compound-nucleus angular momentum; and

$$B_L = \sum_{I_1I_2J} \tfrac{1}{4}(-1)^{S_2-S_1}Z'(l_1Jl_1J;S_1L) \times Z'(l_2Jl_2J;S_2L)\,|U^J_{I_2I_1}|^2$$

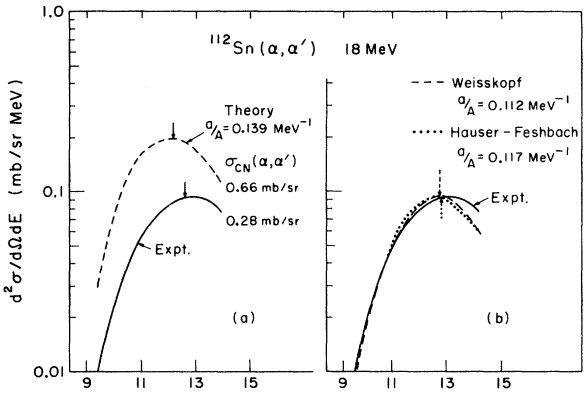

FIG. 4. (a) Comparison of experiment with Weisskopf theory for ^{112}Sn. The Gilbert-Cameron value $a/A=0.139$ MeV^{-1} is used for the theoretical curve. (b) Best values of the level-density parameter a for ^{112}Sn in the Weisskopf and Hauser-Feshbach theories.

with Z' defined in terms of the Racah coefficient W and the Clebsch-Gordan coefficient $(a0c0\,|\,f0)$ by

$$Z'(abcd;ef) = \hat{a}\hat{b}\hat{c}\hat{d}\,(a0c0\,|\,f0)W(abcd;ef)$$

and $|U^J_{I_2I_1}|^2$ is the collision matrix element

$$|U^J_{I_2I_1}|^2 = \frac{T^J_{I_1}(E_{in})T^J_{I_2}(E)}{\sum_{b'I_2'S_2'I_2'}\int_0^{E_{b'y}} dU_{b'}T^J_{b'I_b'}(E')\omega_{b'}(U_{b'},I_2')},$$

where the sum over b' is over all competing channels, the $T^J_{I_1}$, $T^J_{I_2}$ are the transmission coefficients, and the notation $\hat{I}\equiv(2I+1)^{1/2}$.

Both Weisskopf and Hauser-Feshbach theories give the same ^{112}Sn(α, α') CN spectrum to within ~4%, so it is a matter of preference which one we choose to compare with experiment. Figure 4(a) shows how experiment compares with Weisskopf theory. Agreement is not excellent: the positions of the peaks differ by about 0.8 MeV and the magnitudes differ by a factor of 2. This is approximately the same kind of agreement obtained for ^{112}Sn in the (p, α) reactions, but is much better than the results obtained for the heavier isotopes.[1]

In Fig. 4(b) we show the results of our attempt

TABLE II. $Q(\alpha,n)$ in MeV for Ni and Zn isotopes (for Sn isotopes, see Fig. 2).

Target	$Q(\alpha,n)$	Target	$Q(\alpha,n)$
^{58}Ni	−9.3	^{64}Zn	−9.2
^{60}Ni	−7.90	^{66}Zn	−7.44
^{62}Ni	−6.48	^{68}Zn	−5.75
^{64}Ni	−4.88	^{70}Zn	−3.91

TABLE III. Gilbert and Cameron parameters used in calculating theoretical CN cross sections. a/A is the level density parameter in MeV^{-1}, U_0 is the pairing energy in MeV.

Reaction	a/A	U_0	Reaction	a/A	U_0
$^{112}Sn(\alpha,n)^{115}Te$	0.155	1.14	$^{58}Ni(\alpha,n)^{61}Zn$	0.105	1.06
$^{112}Sn(\alpha,p)^{115}Sb$	0.149	1.14	$^{58}Ni(\alpha,p)^{61}Cu$	0.110	1.29
$^{112}Sn(\alpha,\alpha')^{112}Sn$	0.139	2.44	$^{58}Ni(\alpha,\alpha')^{58}Ni$	0.094	2.47
$^{114}Sn(\alpha,n)^{117}Te$	0.158	1.14	$^{60}Ni(\alpha,n)^{63}Zn$	0.118	1.06
$^{114}Sn(\alpha,p)^{117}Sb$	0.151	1.32	$^{60}Ni(\alpha,p)^{63}Cu$	0.123	1.41
$^{114}Sn(\alpha,\alpha')^{114}Sn$	0.143	2.33	$^{60}Ni(\alpha,\alpha')^{60}Ni$	0.109	2.49
$^{116}Sn(\alpha,n)^{119}Te$	0.158	1.14	$^{62}Ni(\alpha,n)^{65}Zn$	0.132	1.06
$^{116}Sn(\alpha,p)^{119}Sb$	0.148	1.15	$^{62}Ni(\alpha,p)^{65}Cu$	0.134	1.50
$^{116}Sn(\alpha,\alpha')^{116}Sn$	0.145	2.51	$^{62}Ni(\alpha,\alpha')^{62}Ni$	0.122	2.61
$^{118}Sn(\alpha,n)^{121}Te$	0.152	1.14	$^{64}Ni(\alpha,n)^{67}Zn$	0.140	1.06
$^{118}Sn(\alpha,p)^{121}Sb$	0.141	1.24	$^{64}Ni(\alpha,p)^{67}Cu$	0.141	1.50
$^{118}Sn(\alpha,\alpha')^{118}Sn$	0.142	2.34	$^{64}Ni(\alpha,\alpha')^{64}Ni$	0.133	2.70
$^{120}Sn(\alpha,n)^{123}Te$	0.145	1.14	$^{64}Zn(\alpha,n)^{67}Ge$	0.142	1.36
$^{120}Sn(\alpha,p)^{123}Sb$	0.129	1.43	$^{64}Zn(\alpha,p)^{67}Ga$	0.141	1.50
$^{120}Sn(\alpha,\alpha')^{120}Sn$	0.135	2.43	$^{64}Zn(\alpha,\alpha')^{64}Zn$	0.125	2.47
$^{122}Sn(\alpha,n)^{125}Te$	0.130	1.14	$^{66}Zn(\alpha,n)^{69}Ge$	0.150	1.36
$^{122}Sn(\alpha,p)^{125}Sb$	0.117	1.09	$^{66}Zn(\alpha,p)^{69}Ga$	0.148	1.50
$^{122}Sn(\alpha,\alpha')^{122}Sn$	0.123	2.62	$^{66}Zn(\alpha,\alpha')^{66}Zn$	0.136	2.56
$^{124}Sn(\alpha,n)^{127}Te$	0.120	1.14	$^{68}Zn(\alpha,n)^{71}Ge$	0.155	1.36
$^{124}Sn(\alpha,p)^{127}Sb$	0.107	1.20	$^{68}Zn(\alpha,p)^{71}Ga$	0.151	1.43
$^{124}Sn(\alpha,\alpha')^{124}Sn$	0.111	2.28	$^{68}Zn(\alpha,\alpha')^{68}Zn$	0.143	2.56
			$^{70}Zn(\alpha,n)^{73}Ge$	0.156	1.36
			$^{70}Zn(\alpha,p)^{73}Ga$	0.150	1.88
			$^{70}Zn(\alpha,\alpha')^{70}Zn$	0.147	2.49

to get a best fit to the experimental results by varying the level density parameter a while keeping the pairing energy fixed. For the Weisskopf theory, the value $a/A = 0.112$ MeV^{-1} (which differs by 20% from the Gilbert-Cameron value of $a/A = 0.139$ MeV^{-1}) gives the best fit, and for the Hauser-Feshbach theory, the value $a/A = 0.117$ MeV^{-1} (15% from the Gilbert-Cameron value) gives the best fit, although in both cases the fit becomes worse as the center of mass (c.m.) energy goes up, the theoretical curves dropping below the experimental curve above c.m. energy of ~12.5 MeV.

It may seem surprising at first that the two theories, which agree so closely when the Gilbert-Cameron parameters are used, should give "best fits" with different values of a/A, but all this really means is that the cross sections given by the two theories do not depend on the level density parameter a in the same way. However, this does suggest the interesting conjecture that the Gilbert-Cameron values for the level density parameters are those values of a/A which will give the closest agreement between the cross sections as calculated by the full angular-momentum dependent (Hauser-Feshbach) theory and the angular-momentum-averaged (Weisskopf) theory.

B. Zn isotopes

Figure 5 shows theoretical Zn(α, α') CN cross-section curves for both Weisskopf and Hauser-Feshbach calculations, where we used the McFadden-Satchler α-particle optical model parameters for Cu since no numbers were available for Zn. The theoretical spectra obtained agree within 30%, and the Hauser-Feshbach theory, being more correct than the Weisskopf theory, is chosen for comparison with the experimental results. This choice did not matter in the case of ^{112}Sn, where the two theoretical curves were identical to within 5%.

The case of the Zn isotopes was complicated by the fact that our ^{70}Zn target had the following composition: 67.56% ^{70}Zn, 12.73% ^{64}Zn, 9.44% ^{68}Zn, 8.05% ^{66}Zn, 2.22% ^{67}Zn. This necessitated a simple correction to the experimental data, a subtraction procedure after which the results were essentially similar to those for Sn, namely, the ^{68}Zn and ^{70}Zn spectra were equal to within ~40%, which is a very reasonable number considering the relative crudeness of the subtraction procedure. As previously mentioned, this equality is strong evidence for the claim that both the ^{68}Zn and ^{70}Zn spectra are almost purely non-CN in nature, and

we can subtract it from the ^{64}Zn and ^{66}Zn spectra to get the CN contributions to the latter isotopes. This is how the experimental curves in Fig. 6(a) are obtained.

This claim that the ^{68}Zn and ^{70}Zn spectra are non-CN in nature would be even more strongly bolstered if the theoretically predicted CN contributions to the ^{68,70}Zn spectra were small compared to the total experimental spectra. While this is true for ^{70}Zn (the theoretical Hauser-Feshbach CN spectrum for ^{70}Zn given in Fig. 5 is about 20% of the experimental total ^{70}Zn spectrum), unfortunately it does not quite hold in the (more accurately measured) case of ^{68}Zn, where the theoretical Hauser-Feshbach CN spectrum shown in Fig. 5 is approximately 80% of the total measured ^{68}Zn spectrum. The extreme case occurs when we assume that the ^{68}Zn spectrum is *all* CN; then no subtraction is done on the ^{64,66}Zn spectra and the experimental curves of Fig. 6(b) are obtained. These experimental curves are thus the experimentally obtained total cross sections for ^{64,66}Zn(α, α') at 18 MeV, after the impurity peaks have been subtracted out and the spectra smoothed for easier comparison with the theoretical curves. The true CN contribution to the ^{64,66}Zn spectra thus will lie somewhere between the two extremes represented by the experimental curves of Figs. 6(a) and 6(b), a difference of less than 10% for ^{64}Zn and about 25% for ^{66}Zn. The shape of the curve and the peak positions are essentially the same in both extremes, however.

Comparison with theory is easy in the case of Fig. 6(b): The experimental curves are compared directly with the Hauser-Feshbach theoretical curves of Fig. 5. The case of Fig. 6(a), where the experimental ^{68}Zn spectrum is subtracted from the ^{64,66}Zn spectra is more subtle; subtracting out the ^{68}Zn total experimental spectrum means that any CN contribution to the ^{68}Zn spectrum is also subtracted out. Thus in order to compare with theory, we subtract the theoretical ^{68}Zn CN spectrum from the theoretical ^{64,66}Zn CN spectra in Fig. 5. It is these subtracted theoretical spectra that are compared to the subtracted experimental spectra in Fig. 6(a).

We see from Fig. 6 that for ^{64}Zn, where the data are most accurate, theory and experiment agree to within 30% in the case with subtraction, and to within 35% in the case without subtraction, while for ^{66}Zn, theory and experiment agree to within 40% in both cases.

C. Ni isotopes

Theoretical curves using both Weisskopf and Hauser-Feshbach theories for Ni(α, α') are shown in Fig. 8. The agreement is again within 30%, and we use the Hauser-Feshbach theory in the comparison with experiment below. The most interesting aspect of these curves is the theoretical prediction that in spite of a large difference in their Q values for the competing (α,n) channel (see Table II), the ^{58}Ni and ^{60}Ni should very closely coincide, an effect that is due to the shell correction to

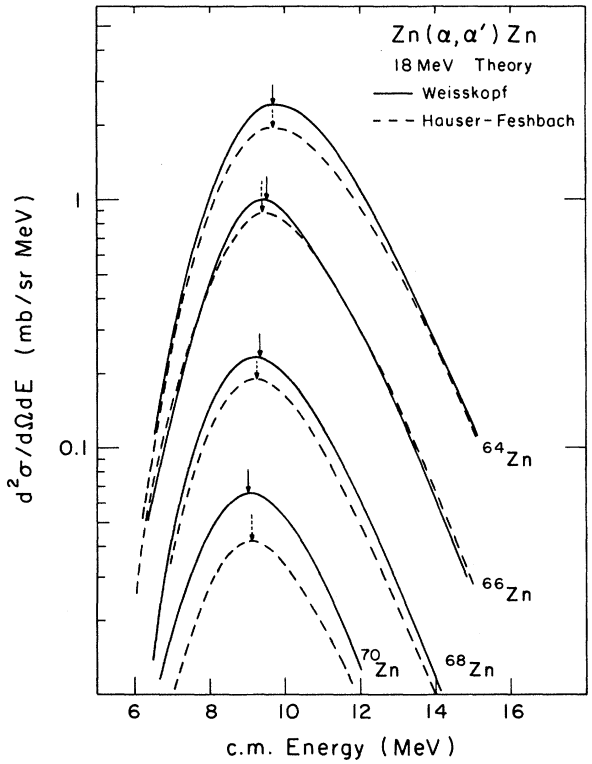

FIG. 5. Theoretical curves for Zn isotopes. Arrows point out the positions of the peaks.

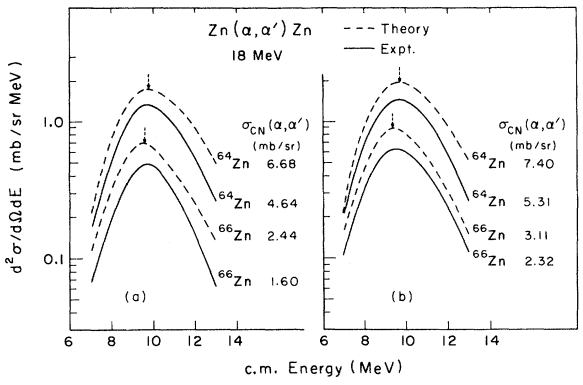

FIG. 6. Comparison between theory and experiment for the Zn isotopes: (a) with subtraction of the ^{68}Zn spectrum, and (b) without subtraction of the ^{68}Zn spectrum.

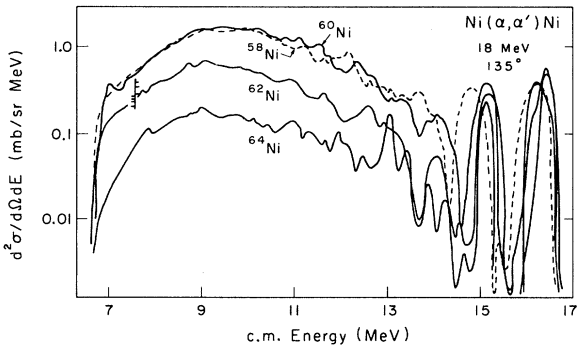

FIG. 7. Raw spectra for Ni(α, α'). The marks at about 8 MeV represent monitor counts taken during the runs of the different Ni isotopes.

the level densities. This is an effect that is not predicted for (α, p) reactions on Ni.

Figure 7 is a plot of typical Ni(α, α')Ni experimental spectra after carbon and oxygen impurities have been subtracted out. The ^{58}Ni and ^{60}Ni spectra are essentially identical just as theory predicts. Smoothing out this experimental spectra gives us the experimental curves of Fig. 9(b), which are compared directly with the appropriate theoretical curves from Fig. 8, also reproduced in Fig. 9(b) for ease of comparison. If we now take the ^{64}Ni spectrum to be the non-CN contribution common to the three other isotopes ^{58,60,62}Ni and subtract it out, we get the experimental spectra shown in Fig. 9(a). As in the case of the Zn isotopes, the theoretical CN spectrum for ^{64}Ni of Fig. 8 is subtracted from the theoretical curves of the other isotopes on the same figure to get the theoretical curves of Fig. 9(a), which are now compared with the experimental curves with subtraction. As in the case of Zn, the true CN spectra for these Ni

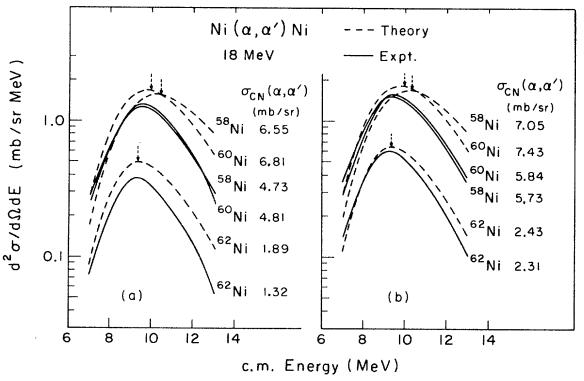

FIG. 9. Comparison between theory and experiment for the Ni isotopes: (a) with subtraction of the ^{64}Ni spectrum, and (b) without subtraction of the ^{64}Ni spectrum.

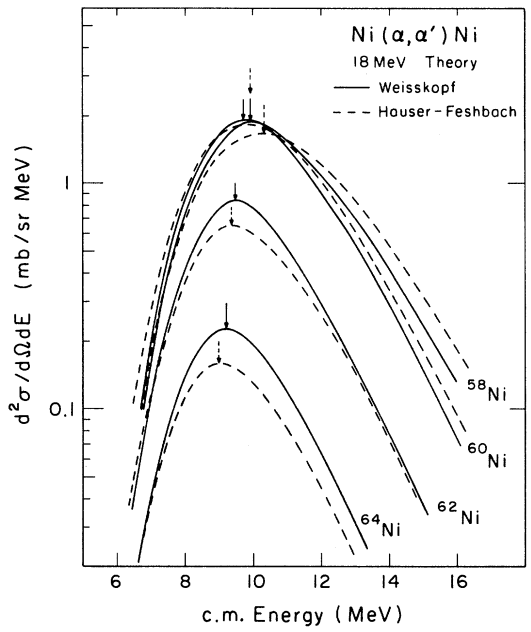

FIG. 8. Theoretical curves for Ni isotopes. Arrows point out the positions of the peaks.

isotopes will be between the extremes represented by the experimental curves of Fig. 9(a) and (b).

To justify taking the total ^{64}Ni spectrum as the non-CN contribution, we compared it with those for ^{68}Zn and ^{70}Zn, which we felt reasonably sure were mostly non-CN in nature. The ^{64}Ni spectrum

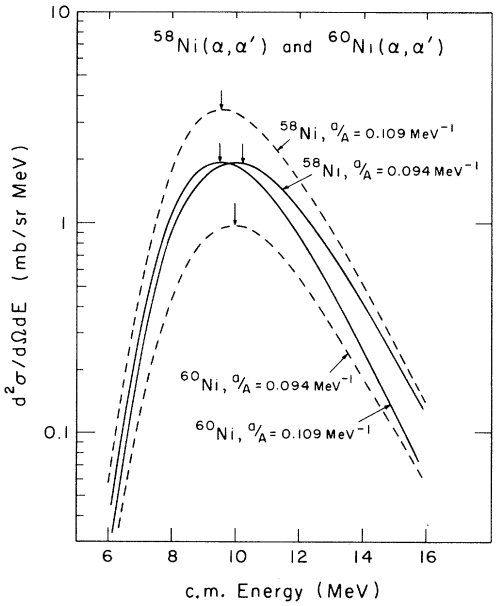

FIG. 10. Theoretical plots (Weisskopf theory) showing the effect of the level density parameter in bringing the CN spectra of the ^{58,60}Ni isotopes together.

agreed with the ^{68}Zn spectrum within 40%. Since non-CN reactions for nearby nuclei will not differ radically, this result provides some justification for using our method here. On the other hand, the theoretical ^{64}Ni CN spectrum (Fig. 8) is almost 75% of the total experimental ^{64}Ni α spectrum, so the evidence that our ^{64}Ni spectrum is indeed non-CN in nature is much weaker than in the other two cases (Sn and Zn). This may explain why agreement between theory and experiment is better when no subtraction is performed [Fig. 9(b): differences between theory and experiment are about 20% for ^{58}Ni, 25% for ^{60}Ni, and 5% for ^{62}Ni], than when the ^{64}Ni spectrum is subtracted off. (33% for ^{58}Ni and 35% for both ^{60,62}Ni.) In both cases, though, the agreement between theory and experiment for the positions of the spectra peaks is relatively poor for the lighter isotopes (about 0.9 MeV for ^{58}Ni and 0.5 MeV for ^{60}Ni) but excellent for ^{62}Ni. This is because the peaks in the *experimental* spectra tend to occur at the same c.m. energy for various isotopes of the same element, while according to theory, the peak position should shift to lower c.m. energy as one goes to heavier isotopes.

The surprising experimental confirmation of the theoretical prediction that the ^{58,60}Ni spectra coincide was investigated further by varying the values of the shell parameter a/A for both isotopes from the values given by Gilbert and Cameron. Since there is no canonical way to choose new values for a/A, we simply interchanged the values for the two isotopes, that is: Gilbert and Cameron give values of $a/A = 0.094$ MeV^{-1} for ^{58}Ni and $a/A = 0.109$ MeV^{-1} for ^{60}Ni; we interchanged these numbers and plotted CN cross-section curves using the value $a/A = 0.109$ MeV^{-1} for ^{58}Ni and $a/A = 0.094$ for ^{60}Ni. The resulting curves are shown as dashed lines in Fig. 10, where it is clear that interchanging the values of a/A decreases the cross section for ^{60}Ni and increases that for ^{58}Ni, aside from shifting the positions of the peak somewhat. This experimental verification represents an important success for the Gilbert-Cameron level density parameters.

Finally, experimental results were isotropic to within 30%, and were consistently lower than theoretical predictions as can be seen from the figures.

---

†Work supported by the National Science Foundation.

[1]B. L. Cohen, G. R. Rao, C. L. Fink, J. C. Van der Weerd, and J. A. Penkrot, Phys. Rev. Lett. 25, 306 (1970); G. R. Rao, R. Balasubramanian, B. L. Cohen, C. L. Fink, and J. H. Degnan, Phys. Rev. C 4, 1855 (1971); K. C. Chan, G. R. Rao, B. L. Cohen, J. H. Degnan, and L. Shabason, *ibid.* 8, 1363 (1973); the (α, p) results are unpublished.

[2]F. G. Perey, Phys. Rev. 131, 745 (1963).

[3]L. McFadden and G. R. Satchler, Nucl. Phys. 84, 177 (1966).

[4]A. Gilbert and A. G. W. Cameron, Can. J. Phys. 43, 1446 (1965).

[5]J. M. Blatt and V. F. Weisskopf, *Theoretical Nuclear Physics* (Wiley, New York, 1952).

[6]A. C. Douglas and N. MacDonald, Nucl. Phys. 13, 382 (1959).